

LaST₀: Latent Spatio-Temporal Chain-of-Thought for Robotic Vision-Language-Action Model

Zhuoyang Liu^{*1,2,4}, Jiaming Liu^{*†1,4}, Hao Chen^{*3,4}, Jiale Yu¹, Ziyu Guo³, Chengkai Hou^{1,2}, Chenyang Gu¹, Xiangju Mi¹, Renrui Zhang³, Kun Wu², Zhengping Che^{†2}, Jian Tang², Pheng-Ann Heng³, Shanghang Zhang^{✉1}

¹State Key Laboratory of Multimedia Information Processing, School of Computer Science, Peking University

²Beijing Innovation Center of Humanoid Robotics ³CUHK ⁴Simplexity Robotics

Project page: <https://vla-last0.github.io/>

*Equal Contribution †Project Lead ✉Corresponding Author

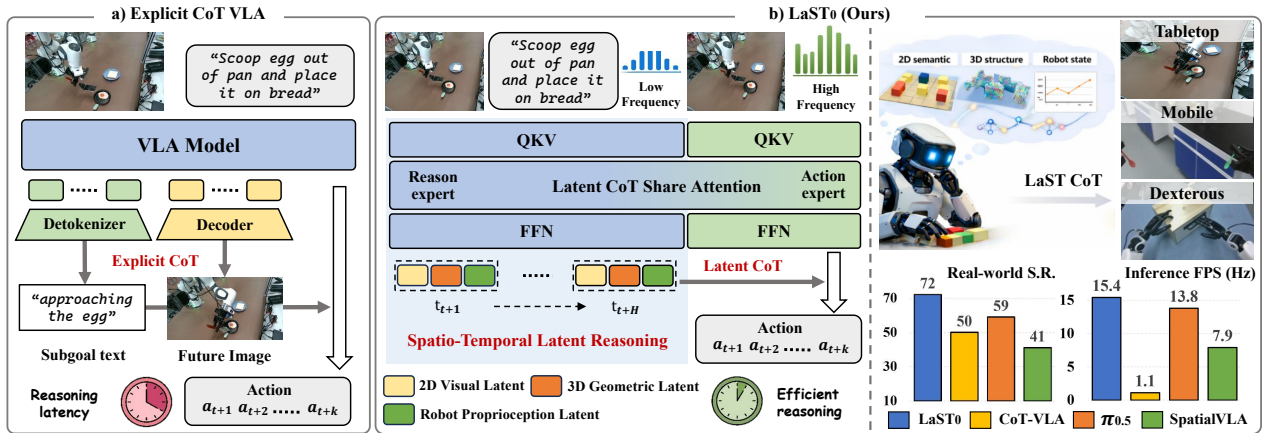


Figure 1. Overview. (a) Unlike previous VLA methods that explicitly generate linguistic reasoning traces or future visual observations, (b) we propose LaST₀, a framework that enables efficient reasoning before acting through a Latent Spatio-Temporal CoT. This latent CoT captures multimodal physical and robotic dynamics that are difficult to verbalize and propagates them over time to form temporally consistent reasoning. LaST₀ achieves SOTA performance across a wide range of tasks while enabling more efficient model inference.

Abstract

Vision-Language-Action (VLA) models have recently shown strong generalization, with some approaches seeking to explicitly generate linguistic reasoning traces or predict future observations prior to execution. However, explicit reasoning typically incurs non-negligible inference latency, which constrains the temporal resolution required for robotic manipulation. Moreover, such reasoning is confined to the linguistic space, imposing a representational bottleneck that struggles to faithfully capture ineffable physical attributes. To mitigate these limitations, we propose **LaST₀**, a framework that enables efficient *reasoning before acting* through a Latent Spatio-Temporal Chain-of-Thought (CoT), capturing fine-grained physical and robotic dynamics that are often difficult to verbalize. Specifically, we introduce a token-efficient latent CoT space that models future visual dynamics, 3D structural information, and robot proprioceptive states, and

further extends these representations across time to enable temporally consistent implicit reasoning trajectories. Furthermore, LaST₀ adopts a dual-system architecture implemented via a Mixture-of-Transformers design, where a reasoning expert conducts low-frequency latent inference and an acting expert generates high-frequency actions conditioned on robotics-oriented latent representations. To facilitate coordination, LaST₀ is trained with heterogeneous operation frequencies, enabling adaptive switching during deployment. Across 10 real-world tasks spanning tabletop, mobile, and dexterous hand manipulation, LaST₀ improves mean success rates by 13%, 14% and 14% over prior SOTA VLA methods, respectively.

1. Introduction

By inheriting the semantic understanding and common-sense reasoning capabilities of Vision-Language Models (VLMs) (Alayrac et al., 2022; Karamcheti et al., 2024; Deng

et al., 2025a), Vision-Language-Action (VLA) models integrate rich pretrained knowledge with the low-level control capabilities of robotic policies (Brohan et al., 2023; Black et al., 2024; Intelligence et al., 2025). This integration endows robotic agents with a unified framework for interpreting human instructions and executing corresponding manipulation primitives in dynamic environments.

Rather than simply mapping observations to actions, recent advances in VLA models have been inspired by the Chain-of-Thought (CoT) reasoning paradigm in general VLMs (Guo et al., 2025). In this line of work, some approaches enhance manipulation stability and interpretability by explicitly generating linguistic reasoning traces or affordance representations (Ye et al., 2025; Li et al., 2025a). In parallel, other studies seek to capture environmental dynamics by predicting future states (Tian et al., 2024; Zhang et al., 2025b; Wang et al., 2025c; Zhao et al., 2025). Despite their demonstrated benefits, explicit CoT VLA methods remain constrained by two fundamental challenges in robotic manipulation. **On the one hand**, explicit reasoning typically incurs non-negligible inference latency. The autoregressive generation paradigm introduces inevitable computational overhead (Tan et al., 2025; Wang et al., 2025b), limiting the VLA model’s ability to achieve real-time responsiveness. This latency further restricts VLA models from reasoning effectively along the temporal dimension, thereby undermining the temporal consistency required for closed-loop manipulation. **On the other hand**, explicit reasoning is often confined to the linguistic space, imposing a representational bottleneck that struggles to faithfully capture ineffable physical attributes. In contrast, robotic agents must reason about and interact with the physical world, which is essential for robust manipulation in a dynamic environment.

In this paper, we propose **LaST₀**, a dual-system VLA model that enables efficient reason-before-act behavior through a **Latent Spatio-Temporal Chain-of-Thought (CoT)**. As shown in Fig. 1, unlike prior explicit CoT-based VLA methods, LaST₀ performs reasoning in a compact latent space, enabling the capture of fine-grained physical and robotic dynamics that are difficult to verbalize, while supporting temporally coherent modeling. Specifically, we introduce a token-efficient latent CoT space that autoregressively predicts future latent tokens of 2D images, 3D point clouds, and proprioceptive states. As a result, the VLA model can implicitly model the semantic and geometric structure of physical dynamics, while forming an internal representation of the robot state, thereby capturing the relationship between the robot and its interactive environment. Meanwhile, the latent CoT space is extended across future keyframes, enabling temporally consistent causal reasoning, which improves action coherence in closed-loop robotic manipulation. Although the proposed latent CoT is compact and encodes richer physical information, incorporating it into action gen-

eration still introduces additional inference overhead. Therefore, leveraging temporally extended latent conditions, we further propose a dual-system architecture implemented via a Mixture-of-Transformers (MoT) design. Specifically, two experts are integrated within a single VLA model: a slow reasoning expert, which performs low-frequency latent inference to capture spatio-temporal dependencies, and a fast acting expert, which generates actions conditioned on high-frequency observations and periodically updated latent representations. Through shared self-attention mechanisms, LaST₀ enables long-context interaction between the latent CoT space and the action space, thereby effectively coordinating deliberative reasoning with responsive control.

For the training procedure, both the latent reasoning expert and the action expert are initialized from the same pretrained VLM (i.e., Janus-Pro (Chen et al., 2025b)). We then perform large-scale pretraining of LaST₀ on diverse robotic manipulation datasets (Open X-Embodiment Collaboration et al., 2023; Khazatsky et al., 2024; Wu et al., 2025; Hou et al., 2025), ensuring seamless interaction between the two experts within a unified VLA model. During downstream training, we jointly optimize the two experts, with the action expert trained under heterogeneous fast-slow operating ratios, enabling the VLA model to adaptively select appropriate execution frequencies during deployment. For evaluation, we systematically assess LaST₀ on 10 simulated tasks and 10 complex real-world tasks spanning tabletop single- and dual-arm, mobile, and dexterous hand manipulation, where it outperforms prior SOTA VLA methods by 8% in simulation and by 13%, 14%, and 14% across three real-world scenarios, respectively, while achieving a 14× speedup over previous explicit CoT VLA approaches. In addition, we validate the manipulation capability of LaST₀ on long-horizon real-world tasks, such as repeatedly scooping eggs from a pan while adapting to dynamic environmental changes. **Our contributions are summarized as follows:**

- We propose **LaST₀**, a unified VLA model that enables efficient reason-before-act behavior through a **Latent Spatio-Temporal CoT**, performing reasoning in a compact latent space to capture fine-grained physical and robotic dynamics that are difficult to verbalize.
- We design a spatio-temporal latent CoT space, which autoregressively models future semantic, geometric, and proprioceptive information, allowing **LaST₀** to reason about physical dynamics in a temporally coherent manner.
- We introduce a dual system VLA architecture, implemented via MoT scheme, that coordinates low-frequency latent reasoning with high-frequency action generation, enabling real-time robotic manipulation.

2. Related Work

Vision-Language-Action (VLA) Model. VLA models are primarily driven by scaling robot demonstration data and

adapting pretrained VLMs for robotic control (Belkhale et al., 2024; Li et al., 2023; Kim et al., 2024). To improve expressivity for continuous actions, recent VLA research has increasingly employed continuous generative policy heads. Diffusion-based VLA (Wen et al., 2024; 2025b; Liu et al., 2025a) models complex action distributions through iterative denoising, while flow-matching formulations (Intelligence et al., 2025; Deng et al., 2025c; Bjorck et al., 2025; Wen et al., 2025a) offer an alternative that can improve sampling efficiency and stability. Meanwhile, recent research equips VLA models with “reason-before-act” components to improve physical world reasoning. (Intelligence et al., 2025; Lin et al., 2025; Zawalski et al., 2025) adopts textual chain-of-thought (CoT) generation for future task planning and action generation. Subsequent work (Wang et al., 2025d; Zhao et al., 2025; Chen et al., 2025a; Gao et al., 2025; Bu et al., 2025; Zhang et al., 2025b) extends generative text planning to future image prediction. Furthermore, (Liu et al., 2025b; Cen et al., 2025; Gu et al., 2025) introduces predictions of future multi-modal information. However, explicit reasoning typically incurs non-negligible inference latency. LaST₀ proposes a latent CoT strategy to efficiently capture fine-grained physical and robotic dynamics within a compact latent space.

Latent CoT. Recent work of VLM in the general domain (Chen et al., 2025c; Deng et al., 2024; Hao et al., 2024; Yang et al., 2025; Wang et al., 2025b; Li et al., 2025b) has explored latent CoT reasoning to address the limitations of explicit CoT on ineffable visual-spatial matching and high-cost generation. These methods perform multi-step inference directly in continuous latent spaces, allowing intermediate reasoning to be compact, implicit, and tightly integrated with downstream prediction. Beyond general-purpose VLMs, similar approaches have been adopted in the embodied intelligence domain, where textual CoT is particularly ill-suited for representing low-level signal generation. LCDrive (Tan et al., 2025) replaces language-based explanations with action-aligned latent rollouts for autonomous driving. Thinkact (Huang et al., 2025) compresses intermediate motion plans into compact representations. Our proposed LaST₀ is tailored for robotic manipulation, reasoning in a physically grounded latent space that jointly encodes semantic intent, geometric structure, and robot state.

3. Method

3.1. Preliminaries

VLA Problem Formulation. We formulate the robot manipulation task as a probabilistic sequence decision-making problem (Kim et al., 2024). At each timestep t , the policy receives a natural language instruction l_t and visual observations $I_t \in \mathbb{R}^{H \times W \times 3}$ that capture the current environment. The objective of the VLA model π_θ is to generate an opti-

mal action sequence $\mathbf{a}_{t:t+H}$ conditioned on the instruction l_t . We define the action space within the Special Euclidean group $SE(3)$. For single-arm configurations (e.g., Franka research 3), we employ a 7-DoF end-effector pose control mechanism, formulated as $\mathbf{a}_t \in \mathbb{R}^7$. Specifically, this control vector consists of 3-DoF for relative positional offsets ($[\Delta x, \Delta y, \Delta z] \in \mathbb{R}^3$), 3-DoF for rotation (represented as Euler angles [roll, pitch, yaw] $\in \mathbb{R}^3$), and 1-DoF for the gripper state (open/closed, $g \in \mathbb{R}^1$). For dual-arm configurations, we extend the action representation to 14 DoF by concatenating control signals to validate scalability; for mobile manipulation, we additionally estimate the base’s linear and angular velocities. Additional robotic CoT reasoning preliminaries are provided in Appendix F.1.

3.2. LaST₀ Architecture

Overview. As illustrated in Fig. 2 a), we elaborate on the architectural of LaST₀. Our model is initialized on the Janus-Pro(Chen et al., 2025b), utilizing DeepSeek-LLM 1.5B as the backbone. To bridge the gap between reasoning and control, we transform this standard decoder-only transformer into a unified MoT dual-system architecture, constructing the “reason-before-act” paradigm. This design enables the model to effectively decouple the generation of slow, high-level latent reasoning from fast, low-level action execution, while maintaining seamless information flow through a shared attention mechanism.

Vision Encoder. For each input RGB observation $I_t \in \mathbb{R}^{H \times W \times 3}$ ($H = W = 384$), we employ SigLIP-Large(Zhai et al., 2023) to extract semantic features. The encoder yields a compact feature sequence $f_{\text{img}} \in \mathbb{R}^{B \times N_{\text{img}} \times d_v}$, where B denotes the batch size, N_{img} represents the sequence length, and d_v is the embedding dimension. In our framework, these encoded features f_{img} serve a dual purpose: the current frame acts as real-time contextual input to the MoT experts, while future frames provide ground-truth target embeddings for the visual component of the latent CoT.

Point Cloud Encoder (training only). To equip the model with fine-grained geometric perception and robust 3D spatial reasoning, we integrate a large-scale, pretrained point cloud encoder, Uni3D (Zhou et al., 2023b), which explicitly captures object geometry and spatial knowledge. Note that, unlike the vision encoder, the point cloud encoder is not used during inference. Instead, Uni3D is solely employed to encode ground-truth point clouds into compact 3D feature representations within the latent CoT space.

Mixture-of-Transformers LLM Backbone. We adopt DeepSeek-LLM 1.5B as our foundation, repurposing its 24-layer decoder-only transformer architecture into a unified dual-system policy. To efficiently support both high-level reasoning and low-level execution, we transform the standard backbone into a MoT architecture (Deng et al., 2025b).

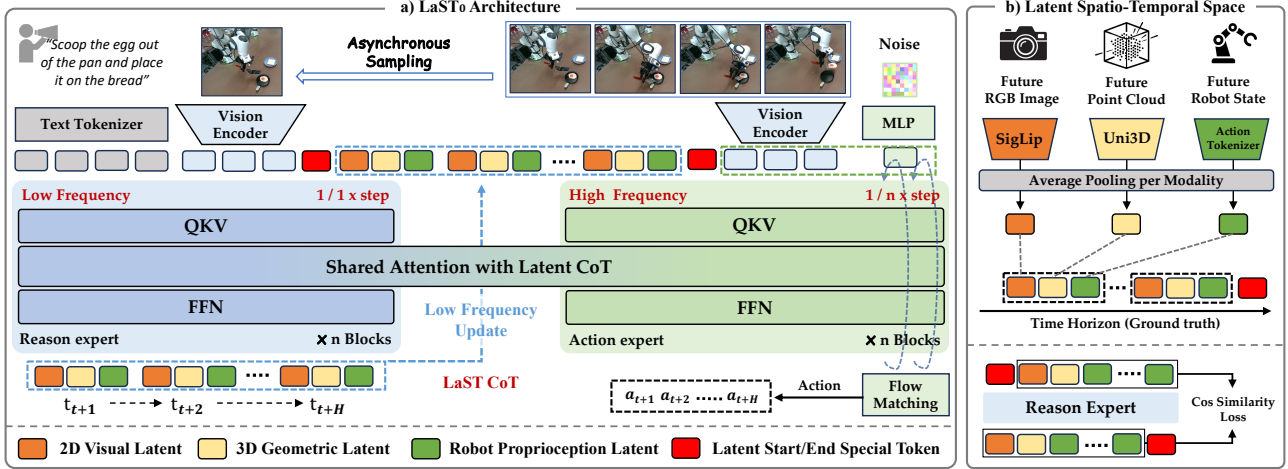


Figure 2. **Framework.** **a)** We propose LaST₀, a unified VLA model with a dual-system architecture. The model is implemented via a MoT scheme with two experts interacting through shared self-attention. The slow reasoning expert operates at a low frequency, taking images and text as input to construct the LaST CoT through autoregression. The fast acting expert operates at a higher frequency and generates actions via flow matching, conditioned on high-frequency observations and periodically updated latent representations. **b)** We design a spatio-temporal latent space, where pretrained modality-specific encoders extract features from future RGB images, point clouds, and robot states. These features serve as ground-truth latent CoT targets for supervising the reasoning expert.

Unlike conventional transformers that apply a homogeneous set of weights to all tokens, our MoT design introduces task-specific parameter sets for all non-embedding components, including Feed-Forward Networks (FFN), attention projections (W_Q, W_K, W_V, W_O), and Layer Normalizations, while maintaining a shared global self-attention context. This modification essentially yields two specialized experts residing within the same $d = 2048$ dimensional latent space, while a slow reasoning expert responsible for autoregressively synthesizing the Latent CoT embeddings \mathcal{Z} from language and slow-stream visual inputs, and a fast acting expert dedicated to generating high-frequency actions \mathbf{a}_t . The design of different operating frequencies for the two experts is described in Section 3.4.

MLP Components. To further clarify the LaST₀ architecture, we describe the remaining auxiliary components, all of which are implemented as Multi-Layer Perceptrons (MLPs). First, a 3D Projector aligns point cloud features to the same dimension, serving as supervise targets for the Latent CoT. Regarding the action generation mechanism, given that our fast acting expert adopts a Flow Matching policy (Black et al., 2024), specific modules are incorporated to handle the continuous generative dynamics. For the action expert input, we use a timestep MLP to encode the continuous time coordinate $t \in [0, 1]$, initialized with sinusoidal embeddings, and a noised-action MLP to project the perturbed action state. For the action expert output, a projector MLP is used to transform the predicted flow velocity field.

3.3. Latent Spatio-Temporal Chain-of-Thought

To capture fine-grained physical and robotic dynamics that are difficult to verbalize, while enabling efficient temporal

modeling for manipulation, we construct a Latent Spatio-Temporal Chain-of-Thought (LaST CoT).

Latent Embedding Construction. To model temporal environmental dynamics, our latent representation encodes multimodal future states over a horizon H . As shown in Fig. 2 b), for each future timestep $k \in \{1, \dots, H\}$, we extract features from three complementary modalities to form a holistic physical representation. Future RGB frames I_{t+k} are encoded into visual latents z_k^v using the frozen SigLIP-Large encoder; simultaneously, future point clouds P_{t+k} are processed by the Uni3D encoder to yield geometric latents z_k^p capturing 3D spatial occupancy, while future robot states \mathbf{s}_{t+k} are transformed into proprioceptive latents z_k^s via an action tokenizer. Together, these representations enable the VLA model to implicitly model the semantic and geometric structure of physical dynamics, while maintaining an internal estimate of the robot’s state, thereby capturing the interaction between the robot and its environment. To ensure high inference efficiency, we apply average pooling to compress the feature maps of each modality into a single representative token. This results in a compact set of embeddings $\{z_k^v, z_k^p, z_k^s\}$ for each step. We then organize these tokens in an interleaved, chronological order to preserve causal physical dependencies:

$$\mathcal{Z}_{\text{GT}} = [z_1^v, z_1^p, z_1^s, z_2^v, z_2^p, z_2^s, \dots, z_H^v, z_H^p, z_H^s]. \quad (1)$$

The interleaved multimodal structure further encourages the model to learn the coupled dynamics across different modalities over time. Notably, the temporal granularity can be flexibly adjusted: we either adopt keyframe extraction as in (Shridhar et al., 2022) or use densely sampled frames, depending on task requirements. Moreover, by compressing

high-dimensional sensory inputs into a latent sequence of length $3 \times H$, we avoid the prohibitive cost of decoding pixel-level images or long textual sequences. In Section 3.4, we introduce an asynchronous frequency design for the two experts, which further accelerates action generation.

Sequence Structure. To better organize LaST CoT reasoning and action generation, we introduce three special tokens: `<latent_start>`, `<latent_end>`, and a placeholder token `<latent_pad>`. The reasoning segment is structurally defined as a sequence bounded by the start and end tokens, with the intermediate positions reserved for the latent embeddings. During Training, we replace the intermediate `<latent_pad>` tokens with the ground-truth latent sequence \mathcal{Z}_{GT} . This allows the model to learn the transition dynamics via standard teacher forcing. While during inference, the model is initialized with `<latent_start>` followed by a sequence of `<latent_pad>` tokens. The slow reason expert then autoregressively generates latent embeddings, sequentially filling the positions of the `<latent_pad>` placeholders until the pre-defined horizon is filled. Horizontal length can be adaptively adjusted and its effect is further analyzed through ablation studies.

Latent Supervision Strategy. Although inference is performed in an autoregressive manner, we train the slow reasoning expert using continuous latent regression rather than discrete token likelihoods (Yang et al., 2025; Wang et al., 2025b). Specifically, the slow expert is trained to predict a sequence of latent reasoning states $\hat{\mathcal{Z}}$ in a next-step prediction manner, conditioned on preceding observations and context. Unlike conventional CoT supervision based on discrete token prediction, our latent targets consist of continuous, high-dimensional embeddings that encode future physical world states. To align the predicted latent with the ground-truth representations, we employ cosine similarity as the supervision objective. The loss is defined as:

$$\mathcal{L}_{\text{latent}} = \sum_{t=1} \left(1 - \frac{\hat{\mathbf{z}}_t \cdot \mathbf{z}_t^{\text{GT}}}{\|\hat{\mathbf{z}}_t\| \|\mathbf{z}_t^{\text{GT}}\|} \right). \quad (2)$$

By maximizing directional alignment in the latent space, this objective encourages the model to anticipate future physical dynamics in a structured and compact manner.

3.4. Dual-System Coordination

Asynchronous Frequency Coordination. To coordinate LaST CoT reasoning with high-frequency robotic control, we introduce an asynchronous frequency mechanism between the slow reasoning expert and the fast acting expert. As shown in Fig. 3, we decouple their operating frequencies using a set of update ratios κ (e.g., $\kappa \in \{2, 4, 8\}$). The slow expert is activated only at sparse keyframes ($t \bmod \kappa = 0$), where it performs autoregressive latent CoT reasoning. In

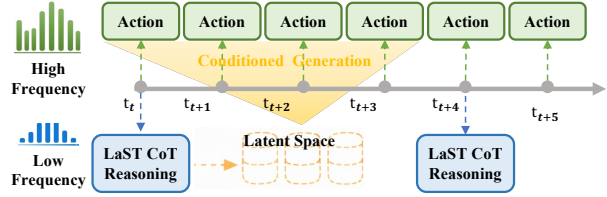


Figure 3. The reasoning expert performs low-frequency latent CoT reasoning to capture spatio-temporal dependencies, while the fast acting expert generates actions conditioned on high-frequency observations and periodically updated latent knowledge.

contrast, the fast expert runs at the native control frequency and remains active at every timestep. Between consecutive keyframes ($t \bmod \kappa \neq 0$), the slow reasoning expert is held dormant, while the fast expert generates actions by conditioning on the most recent latent reasoning output. An interesting empirical finding is that increasing the temporal extent of the latent representations (e.g., by predicting multiple future keyframes) leads to improved performance in action prediction. For the inputs to the two experts, the slow reasoning expert receives the natural language instruction l and the low-frequency observation I_{slow} , constructing the Latent CoT that encapsulates future physical dynamics. Conversely, the fast acting expert is optimized for rapid closed-loop feedback and receives only the high-frequency observation I_{fast} . Crucially, since our MoT architecture maintains a unified token sequence, the fast expert can efficiently attend to both the linguistic goal and the Latent CoT tokens via the shared attention mechanism. The description of the KV cache is provided in Appendix F.2.

3.5. Training Recipe

Large-Scale Robotic Pretraining. First, LaST₀ performs pretraining on a diverse corpus of over 400K trajectories aggregated from Open-X-Embodiment (Open X-Embodiment Collaboration et al., 2023), DROID (Khazatsky et al., 2024), ROBOMIND (Wu et al., 2025), and other robotic datasets. Details are provided in Appendix A.

Supervised Fine-Tuning (SFT). We employ a joint SFT strategy that optimizes both the slow reasoning expert and the fast action expert. Specifically, the slow reasoning expert is trained by minimizing the Latent CoT regression loss $\mathcal{L}_{\text{latent}}$, aligning its latent representations with domain-specific physical dynamics. In parallel, the fast acting expert is optimized using the standard Flow Matching loss $\mathcal{L}_{\text{flow}}$ for action denoising. Meanwhile, the action expert is trained with randomly mixed fast-slow operating ratios (e.g., 1:1, 1:2, 1:4), which exposes it to latent conditions updated at varying delays. As a result, LaST₀ can flexibly accommodate different reasoning-update frequencies at deployment and adaptively choose the fast-slow inference rate. In ablation studies, we find that training with mixed fast-slow operating ratios does not degrade performance; instead, it

improves the model’s robustness during inference.

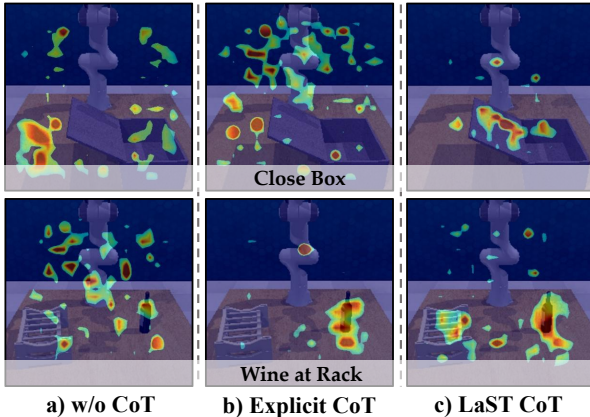


Figure 4. Attention heatmap visualizations from the last layer for three VLA models: (a) LaST₀ without CoT reasoning, (b) the explicit CoT in CoT-VLA, and (c) LaST₀ with LaST CoT.

4. Experiment

Section 4.1 evaluates the manipulation performance and inference efficiency of LaST₀ in simulation, while Section 4.2 conducts the ablation study of each component. Section 4.3 reports results on real-world tasks.

4.1. Simulation Experiment

Data collection. We evaluate LaST₀ on a diverse set of 10 tasks from the RLBench (James et al., 2020) benchmark, conducted in the CoppeliaSim simulation environment. All tasks are executed using a Franka Panda robotic arm with a single front-view observation. Demonstration data are collected by following pre-defined waypoints with motion planner (Sucan et al., 2012). Following the frame-sampling protocol adopted in (Shridhar et al., 2022), we construct a training dataset comprising 100 trajectories per task.

Training and evaluation protocol. We benchmark LaST₀ against six representative state-of-the-art VLA models: OpenVLA (Kim et al., 2024), $\pi_{0.5}$ (Intelligence et al., 2025), CogACT (Li et al., 2024b), SpatialVLA (Qu et al., 2025), CoT-VLA (Zhao et al., 2025) and HybridVLA (Liu et al., 2025a). For all baselines, we initialize from the officially released pretrained checkpoints and follow the full fine-tuning configurations recommended by the paper. For CoT-VLA, we reimplement the method on top of Janus-Pro (Chen et al., 2025b), the same foundation model used in our approach, and reproduce its explicit CoT reasoning to ensure a fair comparison. For LaST₀, each observation consists of a single RGB image resized to 384×384 , a point cloud uniformly subsampled to 1024 points, a language instruction obtained directly from the simulator, and the robot proprioceptive state synchronized with the predicted action. The model is trained for 300 epochs during the SFT stage, using the AdamW optimizer (Loshchilov & Hutter, 2017) across

8 NVIDIA A800 GPUs. Evaluation follows the protocol of prior work (Goyal et al., 2023). For each task, we perform 20 rollout trials using the final checkpoint, repeat the evaluation three times with different random seeds, and report the mean success rate together with its variance.

Quantitative and qualitative analysis. In Table 1, LaST₀-3.3B achieves a mean success rate of 82% across 10 RLBench manipulation tasks. LaST₀ is trained under a mixed fast-slow operating frequency and evaluated at a 1:4 ratio. In particular, LaST₀ surpasses the strongest existing methods, HybridVLA-7B (74%), $\pi_{0.5}$ -3B (65%), and CogACT-7B (61%), by margins of 8%, 17%, and 21%, respectively. Beyond the overall average, LaST₀ attains the highest success rate on 7 out of 10 tasks, indicating consistent performance gains across diverse manipulation skills. These improvements primarily stem from the latent reasoning representations produced by the reasoning expert, which condition the action expert with compact latent states encoding future visual dynamics, 3D spatial structure, and robot proprioceptive information, enabling more stable and temporally coherent action generation. In terms of execution efficiency (without action chunking scheme), LaST₀ operates at an inference speed of 15.4 Hz, which is significantly faster than explicit CoT methods (CoT-VLA: 1.1 Hz) and remains competitive with $\pi_{0.5}$ (13.8 Hz). As shown in Fig. 4, we compare the attention heatmaps of LaST₀ against variants without CoT and with explicit CoT (CoT-VLA). While the no-CoT variant and the explicit CoT method fail to aggregate features over the manipulated objects and the robot, LaST₀ exhibits a highly concentrated attention pattern, highlighting its superior spatio-temporal understanding.

4.2. Ablation Study

To validate the key design choices of LaST₀, we conduct comprehensive ablation experiments on 10 RLBench tasks.

Importance of latent CoT modalities. As shown in Fig. 5(a), we assess each latent modality by ablating individual components while keeping all other parameters fixed at their optimal settings (i.e., latent tokens = 1, temporal coverage = 4). When using only the image, point cloud, or robot state latent, the model achieves success rates of 74%, 76%, and 75%, respectively, indicating that each modality-specific latent provides a strong basis for action generation. The combination of multiple modality latents continues to provide additional performance improvements, even when the manipulation accuracy is already high. These results validate the importance of modeling comprehensive physical dynamics in the latent space, and further demonstrate that enabling the model to autonomously reason about the relationship between the robot and its interactive environment is effective for robotic manipulation.

Number of tokens per latent modality. As shown in Fig. 5

Table 1. Comparison of LaST₀ and baselines on RL-Bench. All methods are trained in the multi-task setting (Shridhar et al., 2022), and we report mean success rates (S.R.). Inference speed is evaluated on an NVIDIA 4090 GPU.

| Models | Close box | Close laptop lid | Toilet seat down | Sweep to dustpan | Close fridge | Phone on base | Umbrella out | Frame off hanger | Wine at rack | Water plants | Mean S.R. ↑ & Var ↓ | Infer. speed ↑ |
|-------------------|-----------|------------------|------------------|------------------|--------------|---------------|--------------|------------------|--------------|--------------|---------------------|----------------|
| OpenVLA | 0.60 | 0.35 | 0.75 | 0.55 | 0.85 | 0.20 | 0.30 | 0.15 | 0.20 | 0.05 | 0.40 ± 0.02 | 6.3 Hz |
| SpatialVLA | 0.80 | 0.70 | 0.85 | 0.20 | 0.80 | 0.15 | 0.25 | 0.40 | 0.15 | 0.30 | 0.46 ± 0.03 | 7.9 Hz |
| CogACT | 0.90 | 0.80 | 0.95 | 0.50 | 0.85 | 0.50 | 0.55 | 0.45 | 0.30 | 0.25 | 0.61 ± 0.04 | 9.8 Hz |
| CoT-VLA | 0.95 | 0.75 | 1.00 | 0.80 | 0.65 | 0.50 | 0.40 | 0.50 | 0.55 | 0.50 | 0.66 ± 0.03 | 1.1 Hz |
| π _{0.5} | 0.90 | 0.95 | 0.85 | 0.75 | 1.00 | 0.05 | 0.10 | 0.80 | 0.75 | 0.35 | 0.65 ± 0.04 | 13.8 Hz |
| HybridVLA | 0.85 | 0.95 | 1.00 | 0.90 | 1.00 | 0.50 | 0.50 | 0.70 | 0.50 | 0.50 | 0.74 ± 0.04 | 6.1 Hz |
| LaST ₀ | 0.95 | 0.95 | 1.00 | 0.80 | 0.85 | 0.75 | 0.75 | 0.70 | 0.85 | 0.60 | 0.82 ± 0.03 | 15.4 Hz |

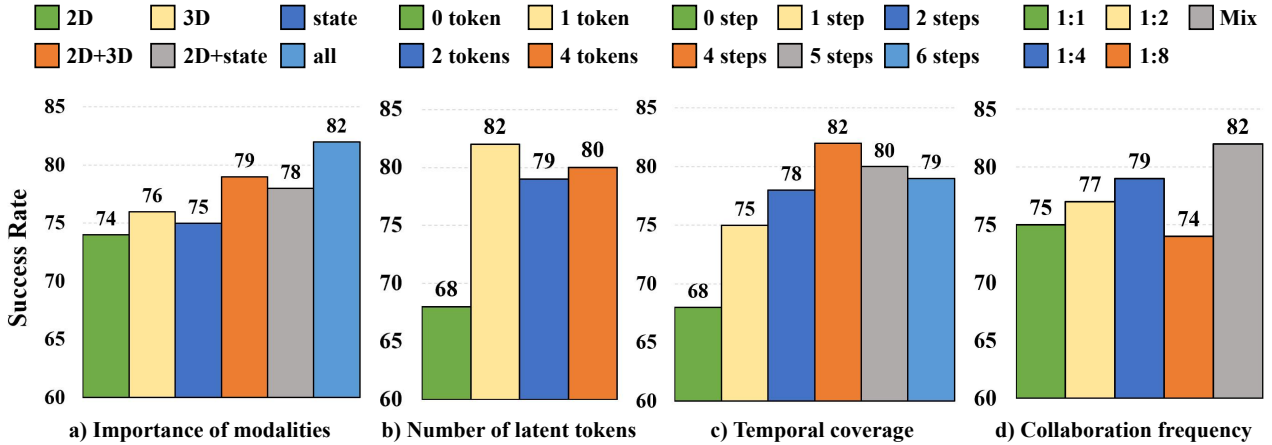


Figure 5. Ablation study on key design choices of LaST₀. We analyze (a) the importance of different latent modalities, (b) the number of tokens allocated per latent modality, (c) the temporal coverage in latent reasoning, and (d) the collaboration frequency between reasoning and action experts. Results are reported as average success rates across 10 RL-Bench tasks.

b), we study how the token budget allocated to each latent modality affects performance by varying the number of latent tokens while keeping other components fixed. When no latent token is used, performance drops substantially to 68%, indicating limited reasoning capacity. Introducing a single token for each modality leads to a sharp improvement (up to 82%), demonstrating that even a minimal latent representation is sufficient to establish an effective latent decision state. Further increasing the number of tokens yields no significant accuracy improvement, suggesting that high-level latent tokens can compactly encode physical information sufficient for effective reasoning.

Temporal coverage in latent reasoning. As shown in Fig. 5 c), we investigate the effect of the temporal horizon used in latent reasoning by varying the number of future time steps encoded into the latent state. Performance improves consistently as the latent temporal coverage increases (from 68% to 82% when extending from 0 to 4 steps), indicating that incorporating longer temporal dependencies enables more informed latent decision states. Since adding further coverage beyond 4 steps does not significantly improve performance, we chose 4 steps as the final latent temporal coverage. The results suggest that extending the temporal horizon of latent prediction beyond that of action prediction is sufficient for improving action generation robustness. Due to our fast-slow system design, extending the tempo-

ral horizon of the latent space does not significantly affect action generation speed.

Collaboration frequency between reasoning and action experts. As shown in Fig. 5 d), varying the collaboration frequency has a clear impact on task success. A series of ratios such as 1:1, 1:2, and 1:4 achieve comparable performance (75-79%), while overly infrequent collaboration (1:8) leads to a relative drop to 74%. Finally, the mixed strategy trained by combining data from all collaboration ratios achieves the best performance (82%), using a 1:4 ratio during testing. These results indicate that our frequency joint training scheme enables more robust coordination between the reasoning and action experts across tasks.

4.3. Real-World Experiment

Data collection. We evaluated our method on a set of real-world manipulation tasks using both single-arm and dual-arm Franka robot setups, as well as AgileX mobile manipulation platforms (Robotics, 2024) and Tien Kung humanoid dexterous hands (Center, 2024). Detailed configurations for different robots and tasks are provided in Appendix B and C. In the single-arm setting, we collect demonstrations for four tasks: 1) *wiping a whiteboard with an eraser*, 2) *pressing a stamp*, 3) *placing a dish on a rack*, and 4) *placing an egg on bread using a spatula*. In addition, we further evaluate a long-horizon setting on *placing egg*

Table 2. Comparison across real-world manipulation tasks. We report success rates (S.R.) for standard single-arm and dual-arm tasks (Franka), mobile manipulation (AgileX), and dexterous manipulation (TienKung). Mean S.R. denotes the average success rate.

| Models | Wipe | Press | Place dish | Place egg | Scoop | Open pot | Mean | Place egg on bread | | | Arrange | Sort | Open | Place |
|-------------------|--------------------|-------------|-------------|-------------|-------------|-------------|-------------|--------------------|-------------|-------------|---------------|-------------|--------------|-------------|
| | whiteboard | stamp | on rack | on bread | popcorn | pick corn | S.R. ↑ | Step 1 | Step 2 | Step 3 | dishes | spoon | drawer | button |
| SpatialVLA | 0.60 | 0.67 | 0.30 | 0.20 | 0.27 | 0.40 | 0.41 | 0.20 | 0.07 | 0.00 | – | – | – | – |
| $\pi_{0.5}$ | 0.60 | 0.73 | 0.60 | 0.47 | 0.53 | 0.60 | 0.59 | 0.47 | 0.20 | 0.07 | 0.47 | 0.20 | 0.67 | 0.53 |
| CoT-VLA | 0.53 | 0.60 | 0.66 | 0.33 | 0.33 | 0.53 | 0.50 | 0.33 | 0.13 | 0.07 | 0.33 | 0.13 | 0.53 | 0.40 |
| LaST ₀ | 0.73 | 0.93 | 0.80 | 0.66 | 0.66 | 0.53 | 0.72 | 0.66 | 0.47 | 0.33 | 0.67 | 0.27 | 0.87 | 0.60 |
| Embodiment | Franka Emika Panda | | | | | | | | | | AgileX Mobile | | TienKung Dex | |

task, where the robot consecutively completes the full task three times while the positions of the manipulated objects continuously change during execution. For the dual-arm setting, two collaborative tasks were considered: 1) *scooping popcorn into a bowl* and 2) *opening a pot lid followed by picking corn from the pot*. For the mobile manipulation task, we evaluate the robot on two tasks: 1) *move to a table and stack plates* and 2) *sort spoons and place them into cabinet*, while for the humanoid robot, we evaluate on 1) *dexterous hand drawer opening* and 2) *dexterous hand place button*. Each task collects 200 teleoperation demonstrations.

Training and evaluation details. We train all policies following the same protocol as in simulation. We compare our method against three strong baselines: $\pi_{0.5}$ (Black et al., 2024), a SOTA 2D VLA model; SpatialVLA (Qu et al., 2025), a SOTA 3D VLA model; and CoT-VLA (Zhao et al., 2025), an explicit CoT-based VLA model that enhances action generation by predicting future visual observations. For fair comparison, all models use the same number of camera viewpoints, and each task is evaluated with 15 rollouts for 3 times under different tabletop positions.

Quantitative and qualitative analysis. As shown in Table 2, LaST₀ achieves the best overall performance on real-world manipulation tasks, with a mean success rate of 72% (± 3) on Franka platform (not including the long-horizon task), substantially outperforming SpatialVLA (41%, ± 2), $\pi_{0.5}$ (59%, ± 4), and CoT-VLA (50%, ± 2). LaST₀ consistently delivers strong gains across a diverse set of tasks, particularly those requiring precise spatial reasoning and temporally coherent control. We further evaluate LaST₀ on a long-horizon manipulation task that requires one, two, and three consecutive successful executions within a single rollout. As shown in Table 2, LaST₀ maintains markedly higher success rates across all stages (0.66 \rightarrow 0.47 \rightarrow 0.33) compared to $\pi_{0.5}$ (0.47 \rightarrow 0.20 \rightarrow 0.07), with the performance gap widening as the horizon increases. This trend indicates that LaST₀ is better able to preserve coherent latent representations of task progress and environment state over extended horizons. Beyond tabletop manipulation, LaST₀ consistently performs precise navigation and coordinated dual-arm control in mobile manipulation tasks, demonstrating that its latent spatio-temporal reasoning generalizes to larger action spaces beyond tabletop settings. For humanoid

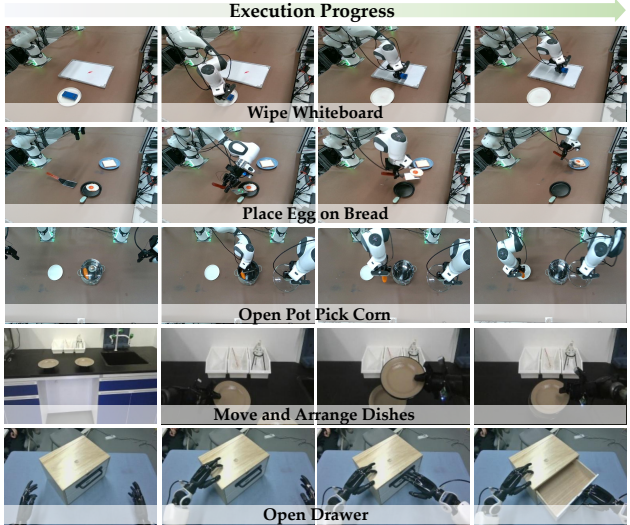


Figure 6. Visualization of Real-World Task Execution.

robots with higher degrees of freedom and dexterous hands, LaST₀ successfully handles complex articulated object manipulation, indicating that its reasoning and action generation capabilities are not constrained by embodiment complexity. We omit comparison with SpatialVLA due to the poor depth estimation. As shown in Fig. 6, we visualize the real-world execution process, with more comprehensive visualizations provided in Appendix D and supplementary video, and failure cases in Appendix E.

5. Conclusion

We introduced LaST₀, a dual-system VLA model that enables efficient reason-before-act behavior for robotic manipulation through a Latent Spatio-Temporal Chain-of-Thought (LaST CoT). By shifting reasoning from explicit traces to a compact latent space, LaST₀ overcomes the latency and representational bottlenecks inherent in prior CoT VLA approaches, while preserving the ability to model fine-grained physical dynamics essential for closed-loop control. Central to our framework is a token-efficient spatio-temporal latent representation that autoregressively captures future semantic, geometric, and proprioceptive dynamics. Building upon this LaST CoT, we further proposed a fast-slow dual-system implemented via a MoT, which decouples low-frequency de-

liberative reasoning from high-frequency action generation. We believe LaST₀ represents a step toward more physically grounded reasoning in robotic foundation models.

Impact Statement

This paper presents work whose goal is to advance the field of Machine Learning. There are many potential societal consequences of our work, none which we feel must be specifically highlighted here.

References

- Alayrac, J.-B., Donahue, J., Luc, P., Miech, A., Barr, I., Hasson, Y., Lenc, K., Mensch, A., Millican, K., Reynolds, M., et al. Flamingo: a visual language model for few-shot learning. *Advances in Neural Information Processing Systems*, 35:23716–23736, 2022.
- Belkhale, S., Cui, Y., and Sadigh, D. Hydra: Hybrid robot actions for imitation learning. *arxiv*, 2023.
- Belkhale, S., Ding, T., Xiao, T., Sermanet, P., Vuong, Q., Tompson, J., Chebotar, Y., Dwibedi, D., and Sadigh, D. Rt-h: Action hierarchies using language, 2024. URL <https://arxiv.org/abs/2403.01823>.
- Bjorck, J., Castañeda, F., Cherniadev, N., Da, X., Ding, R., Fan, L., Fang, Y., Fox, D., Hu, F., Huang, S., et al. Gr00t n1: An open foundation model for generalist humanoid robots. *arXiv preprint arXiv:2503.14734*, 2025.
- Black, K., Brown, N., Driess, D., Esmail, A., Equi, M., Finn, C., Fusai, N., Groom, L., Hausman, K., Ichter, B., et al. pi0: A vision-language-action flow model for general robot control. *arXiv preprint arXiv:2410.24164*, 2024.
- Brohan, A., Brown, N., Carbajal, J., Chebotar, Y., Dabis, J., Finn, C., Gopalakrishnan, K., Hausman, K., Herzog, A., Hsu, J., Ibarz, J., et al. Rt-1: Robotics transformer for real-world control at scale. In *arXiv preprint arXiv:2212.06817*, 2022.
- Brohan, A., Brown, N., Carbajal, J., Chebotar, Y., Chen, X., Choromanski, K., Ding, T., Driess, D., Dubey, A., Finn, C., et al. Rt-2: Vision-language-action models transfer web knowledge to robotic control. In *arXiv preprint arXiv:2307.15818*, 2023.
- Bu, Q., Cai, J., Chen, L., Cui, X., Ding, Y., Feng, S., Gao, S., He, X., Hu, X., Huang, X., et al. Agibot world colosseum: A large-scale manipulation platform for scalable and intelligent embodied systems. *arXiv preprint arXiv:2503.06669*, 2025.
- Cen, J., Yu, C., Yuan, H., Jiang, Y., Huang, S., Guo, J., Li, X., Song, Y., Luo, H., Wang, F., et al. Worldvla: Towards autoregressive action world model. *arXiv preprint arXiv:2506.21539*, 2025.
- Center, T. B. H. R. I. X-humanoid tien kung, 2024. URL <https://x-humanoid.com/>.
- Chen, J., Song, W., Ding, P., Zhou, Z., Zhao, H., Tang, F., Wang, D., and Li, H. Unified diffusion vla: Vision-language-action model via joint discrete denoising diffusion process, 2025a. URL <https://arxiv.org/abs/2511.01718>.
- Chen, L. Y., Adebola, S., and Goldberg, K. Berkeley UR5 demonstration dataset. <https://sites.google.com/view/berkeley-ur5/home>.
- Chen, X., Wu, Z., Liu, X., Pan, Z., Liu, W., Xie, Z., Yu, X., and Ruan, C. Janus-pro: Unified multimodal understanding and generation with data and model scaling. *arXiv preprint arXiv:2501.17811*, 2025b.
- Chen, X., Zhao, A., Xia, H., Lu, X., Wang, H., Chen, Y., Zhang, W., Wang, J., Li, W., and Shen, X. Reasoning beyond language: A comprehensive survey on latent chain-of-thought reasoning. *arXiv preprint arXiv:2505.16782*, 2025c.
- Cui, Z. J., Wang, Y., Shafiqullah, N. M. M., and Pinto, L. From play to policy: Conditional behavior generation from uncurated robot data. *arXiv preprint arXiv:2210.10047*, 2022.
- Dasari, S., Ebert, F., Tian, S., Nair, S., Bucher, B., Schmeckpeper, K., Singh, S., Levine, S., and Finn, C. Robonet: Large-scale multi-robot learning. In *Conference on Robot Learning*, pp. 885–897. PMLR, 2020.
- Dass, S., Yapeter, J., Zhang, J., Zhang, J., Pertsch, K., Nikolaidis, S., and Lim, J. J. CLVR jaco play dataset, 2023. URL https://github.com/clvr-ai/clvr_jaco_play_dataset.
- Deng, C., Zhu, D., Li, K., Gou, C., Li, F., Wang, Z., Zhong, S., Yu, W., Nie, X., Song, Z., Shi, G., and Fan, H. Emerging properties in unified multimodal pretraining, 2025a. URL <https://arxiv.org/abs/2505.14683>.
- Deng, C., Zhu, D., Li, K., Gou, C., Li, F., Wang, Z., Zhong, S., Yu, W., Nie, X., Song, Z., et al. Emerging properties in unified multimodal pretraining. *arXiv preprint arXiv:2505.14683*, 2025b.
- Deng, S., Yan, M., Wei, S., Ma, H., Yang, Y., Chen, J., Zhang, Z., Yang, T., Zhang, X., Zhang, W., et al. Graspvla: a grasping foundation model pre-trained on billion-scale synthetic action data. *arXiv preprint arXiv:2505.03233*, 2025c.

- Deng, Y., Choi, Y., and Shieber, S. From explicit cot to implicit cot: Learning to internalize cot step by step. *arXiv preprint arXiv:2405.14838*, 2024.
- Ebert, F., Yang, Y., Schmeckpeper, K., Bucher, B., Georgakis, G., Daniilidis, K., Finn, C., and Levine, S. Bridge data: Boosting generalization of robotic skills with cross-domain datasets. In *RSS*, 2022.
- Gao, S., Zhou, S., Du, Y., Zhang, J., and Gan, C. Adaworld: Learning adaptable world models with latent actions. *arXiv preprint arXiv:2503.18938*, 2025.
- Goyal, A., Xu, J., Guo, Y., Blukis, V., Chao, Y.-W., and Fox, D. Rvt: Robotic view transformer for 3d object manipulation. In *Conference on Robot Learning*, pp. 694–710. PMLR, 2023.
- Gu, C., Liu, J., Chen, H., Huang, R., Wuwu, Q., Liu, Z., Li, X., Li, Y., Zhang, R., Jia, P., et al. Manualvla: A unified vla model for chain-of-thought manual generation and robotic manipulation. *arXiv preprint arXiv:2512.02013*, 2025.
- Gu, J., Xiang, F., Li, X., Ling, Z., Liu, X., Mu, T., Tang, Y., Tao, S., Wei, X., Yao, Y., Yuan, X., Xie, P., Huang, Z., Chen, R., and Su, H. Maniskill2: A unified benchmark for generalizable manipulation skills, 2023. URL <https://arxiv.org/abs/2302.04659>.
- Guo, D., Yang, D., Zhang, H., Song, J., Zhang, R., Xu, R., Zhu, Q., Ma, S., Wang, P., Bi, X., et al. Deepseek-r1: Incentivizing reasoning capability in llms via reinforcement learning. *arXiv preprint arXiv:2501.12948*, 2025.
- Hao, S., Sukhbaatar, S., Su, D., Li, X., Hu, Z., Weston, J., and Tian, Y. Training large language models to reason in a continuous latent space. *arXiv preprint arXiv:2412.06769*, 2024.
- Heo, M., Lee, Y., Lee, D., and Lim, J. J. Furniturebench: Reproducible real-world benchmark for long-horizon complex manipulation. In *Robotics: Science and Systems*, 2023.
- Hou, C., Wu, K., Liu, J., Che, Z., Wu, D., Liao, F., Li, G., He, J., Feng, Q., Jin, Z., et al. Robomind 2.0: A multimodal, bimanual mobile manipulation dataset for generalizable embodied intelligence. *arXiv preprint arXiv:2512.24653*, 2025.
- Huang, C.-P., Wu, Y.-H., Chen, M.-H., Wang, Y.-C. F., and Yang, F.-E. Thinkact: Vision-language-action reasoning via reinforced visual latent planning. *arXiv preprint arXiv:2507.16815*, 2025.
- Intelligence, P., Black, K., Brown, N., Darpinian, J., Dhabalia, K., Driess, D., Esmail, A., Equi, M., Finn, C., et al. $\pi_{0.5}$: a vision-language-action model with open-world generalization, 2025. URL <https://arxiv.org/abs/2504.16054>.
- James, S., Ma, Z., Arrojo, D. R., and Davison, A. J. Rlbench: The robot learning benchmark & learning environment. *IEEE Robotics and Automation Letters*, 5(2):3019–3026, 2020.
- Jang, E., Irpan, A., Khansari, M., Kappler, D., Ebert, F., Lynch, C., Levine, S., and Finn, C. Bc-z: Zero-shot task generalization with robotic imitation learning. In *Conference on Robot Learning*, pp. 991–1002. PMLR, 2022.
- Kalashnikov, D., Irpan, A., Pastor, P., Ibarz, J., Herzog, A., Jang, E., Quillen, D., Holly, E., Kalakrishnan, M., Vanhoucke, V., et al. QT-Opt: Scalable deep reinforcement learning for vision-based robotic manipulation. *arXiv preprint arXiv:1806.10293*, 2018.
- Karamcheti, S., Nair, S., Balakrishna, A., Liang, P., Kollar, T., and Sadigh, D. Prismatic vlms: Investigating the design space of visually-conditioned language models. In *Forty-first International Conference on Machine Learning*, 2024.
- Khazatsky, A., Pertsch, K., Nair, S., Balakrishna, A., Dasari, S., Karamcheti, S., Nasiriany, S., Srirama, M. K., Chen, L. Y., Ellis, K., Fagan, P. D., Hejna, J., Itkina, M., Lepert, M., Ma, Y. J., Miller, P. T., Wu, J., Belkhale, S., Dass, S., Ha, H., Jain, A., Lee, A., Lee, Y., Memmel, M., Park, S., Radosavovic, I., Wang, K., Zhan, A., Black, K., Chi, C., Hatch, K. B., Lin, S., Lu, J., Mercat, J., Rehman, A., Sanketi, P. R., Sharma, A., Simpson, C., Vuong, Q., Walke, H. R., Wulfe, B., Xiao, T., Yang, J. H., Yavary, A., Zhao, T. Z., Agia, C., Baijal, R., Castro, M. G., Chen, D., Chen, Q., Chung, T., Drake, J., Foster, E. P., Gao, J., Herrera, D. A., Heo, M., Hsu, K., Hu, J., Jackson, D., Le, C., Li, Y., Lin, K., Lin, R., Ma, Z., Maddukuri, A., Mirchandani, S., Morton, D., Nguyen, T., O’Neill, A., Scalise, R., Seale, D., Son, V., Tian, S., Tran, E., Wang, A. E., Wu, Y., Xie, A., Yang, J., Yin, P., Zhang, Y., Bastani, O., Berseth, G., Bohg, J., Goldberg, K., Gupta, A., Gupta, A., Jayaraman, D., Lim, J. J., Malik, J., Martín-Martín, R., Ramamoorthy, S., Sadigh, D., Song, S., Wu, J., Yip, M. C., Zhu, Y., Kollar, T., Levine, S., and Finn, C. Droid: A large-scale in-the-wild robot manipulation dataset. 2024.
- Kim, M. J., Pertsch, K., Karamcheti, S., Xiao, T., Balakrishna, A., Nair, S., Rafailov, R., Foster, E., Lam, G., Sanketi, P., et al. Openvla: An open-source vision-language-action model. *arXiv preprint arXiv:2406.09246*, 2024.
- Kumar, V., Shah, R., Zhou, G., Moens, V., Caggiano, V., Gupta, A., and Rajeswaran, A. Robohive: A unified

- framework for robot learning. In *Thirty-seventh Conference on Neural Information Processing Systems Datasets and Benchmarks Track*, 2023.
- Li, J., Zhu, Y., Tang, Z., Wen, J., Zhu, M., Liu, X., Li, C., Cheng, R., Peng, Y., and Feng, F. Improving vision-language-action models via chain-of-affordance. *arXiv preprint arXiv:2412.20451*, 2024a.
- Li, J., Zhu, Y., Tang, Z., Wen, J., Zhu, M., Liu, X., Li, C., Cheng, R., Peng, Y., Peng, Y., et al. Coa-vla: Improving vision-language-action models via visual-text chain-of-affordance. In *Proceedings of the IEEE/CVF International Conference on Computer Vision*, pp. 9759–9769, 2025a.
- Li, K., Shang, C., Karlinsky, L., Feris, R., Darrell, T., and Herzig, R. Latent implicit visual reasoning, 2025b. URL <https://arxiv.org/abs/2512.21218>.
- Li, Q., Liang, Y., Wang, Z., Luo, L., Chen, X., Liao, M., Wei, F., Deng, Y., Xu, S., Zhang, Y., et al. Cogact: A foundational vision-language-action model for synergizing cognition and action in robotic manipulation. *arXiv preprint arXiv:2411.19650*, 2024b.
- Li, X., Zhang, M., Geng, Y., Geng, H., Long, Y., Shen, Y., Zhang, R., Liu, J., and Dong, H. Manipllm: Embodied multimodal large language model for object-centric robotic manipulation, 2023. URL <https://arxiv.org/abs/2312.16217>.
- Lin, F., Nai, R., Hu, Y., You, J., Zhao, J., and Gao, Y. Onetwovla: A unified vision-language-action model with adaptive reasoning. *arXiv preprint arXiv:2505.11917*, 2025.
- Liu, J., Chen, H., An, P., Liu, Z., Zhang, R., Gu, C., Li, X., Guo, Z., Chen, S., Liu, M., et al. Hybridvla: Collaborative diffusion and autoregression in a unified vision-language-action model. *arXiv preprint arXiv:2503.10631*, 2025a.
- Liu, Z., Liu, J., Xu, J., Han, N., Gu, C., Chen, H., Zhou, K., Zhang, R., Hsieh, K. C., Wu, K., et al. Mla: A multisensory language-action model for multimodal understanding and forecasting in robotic manipulation. *arXiv preprint arXiv:2509.26642*, 2025b.
- Loshchilov, I. and Hutter, F. Decoupled weight decay regularization. *arXiv preprint arXiv:1711.05101*, 2017.
- Luo, J., Xu, C., Liu, F., Tan, L., Lin, Z., Wu, J., Abbeel, P., and Levine, S. FMB: A functional manipulation benchmark for generalizable robotic learning. <https://functional-manipulation-benchmark.github.io>, 2023.
- Lynch, C., Wahid, A., Tompson, J., Ding, T., Betker, J., Baruch, R., Armstrong, T., and Florence, P. Interactive language: Talking to robots in real time. *IEEE Robotics and Automation Letters*, 2023.
- Mandlekar, A., Zhu, Y., Garg, A., Booher, J., Spero, M., Tung, A., Gao, J., Emmons, J., Gupta, A., Orbay, E., Savarese, S., and Fei-Fei, L. RoboTurk: A crowdsourcing platform for robotic skill learning through imitation. *CoRR*, abs/1811.02790, 2018.
- Matsushima, T., Furuta, H., Iwasawa, Y., and Matsuo, Y. Weblab xarm dataset, 2023.
- Mees, O., Borja-Diaz, J., and Burgard, W. Grounding language with visual affordances over unstructured data. In *Proceedings of the IEEE International Conference on Robotics and Automation (ICRA)*, London, UK, 2023.
- Mendonca, R., Bahl, S., and Pathak, D. Structured world models from human videos. *CoRL*, 2023.
- Oh, J., Kanazawa, N., and Kawaharazuka, K. X-embodiment u-tokyo pr2 datasets, 2023. URL https://github.com/ojh6404/rlds_dataset_builder.
- Open X-Embodiment Collaboration, Padalkar, A., Pooley, A., et al. Open X-Embodiment: Robotic learning datasets and RT-X models. <https://arxiv.org/abs/2310.08864>, 2023.
- Padalkar, A., Quere, G., Raffin, A., Silvério, J., and Stulp, F. A guided reinforcement learning approach using shared control templates for learning manipulation skills in the real world. 2023.
- Qu, D., Song, H., Chen, Q., Yao, Y., Ye, X., Ding, Y., Wang, Z., Gu, J., et al. Spatialvla: Exploring spatial representations for visual-language-action model. *arXiv preprint arXiv:2501.15830*, 2025.
- Robotics, A. Agilex cobot magic, 2024. URL <https://global.agilex.ai/products/cobot-magic>.
- Rosete-Beas, E., Mees, O., Kalweit, G., Boedecker, J., and Burgard, W. Latent plans for task agnostic offline reinforcement learning. In *Proceedings of the 6th Conference on Robot Learning (CoRL)*, 2022.
- Shafiqullah, N. M. M., Rai, A., Etukuru, H., Liu, Y., Misra, I., Chintala, S., and Pinto, L. On bringing robots home, 2023.
- Shridhar, M., Manuelli, L., and Fox, D. Perceiver-actor: A multi-task transformer for robotic manipulation. In *Proceedings of the 6th Conference on Robot Learning (CoRL)*, 2022.

- Sucan, I. A., Moll, M., and Kavraki, L. E. The open motion planning library. *IEEE Robotics & Automation Magazine*, 19(4):72–82, 2012.
- Tan, S., Chitta, K., Chen, Y., Tian, R., You, Y., Wang, Y., Luo, W., Cao, Y., Krahenbuhl, P., Pavone, M., et al. Latent chain-of-thought world modeling for end-to-end driving. *arXiv preprint arXiv:2512.10226*, 2025.
- Tian, Y., Yang, S., Zeng, J., Wang, P., Lin, D., Dong, H., and Pang, J. Predictive inverse dynamics models are scalable learners for robotic manipulation, 2024. URL <https://arxiv.org/abs/2412.15109>.
- Walke, H., Black, K., Lee, A., Kim, M. J., Du, M., Zheng, C., Zhao, T., Hansen-Estruch, P., Vuong, Q., He, A., Myers, V., Fang, K., Finn, C., and Levine, S. Bridgedata v2: A dataset for robot learning at scale, 2023.
- Wang, J., Chen, M., Karaev, N., Vedaldi, A., Rupprecht, C., and Novotny, D. Vggt: Visual geometry grounded transformer. In *Proceedings of the Computer Vision and Pattern Recognition Conference*, pp. 5294–5306, 2025a.
- Wang, Q., Shi, Y., Wang, Y., Zhang, Y., Wan, P., Gai, K., Ying, X., and Wang, Y. Monet: Reasoning in latent visual space beyond images and language. *arXiv preprint arXiv:2511.21395*, 2025b.
- Wang, Y., Li, X., Wang, W., Zhang, J., Li, Y., Chen, Y., Wang, X., and Zhang, Z. Unified vision-language-action model. *arXiv preprint arXiv:2506.19850*, 2025c.
- Wang, Y., Li, X., Wang, W., Zhang, J., Li, Y., Chen, Y., Wang, X., and Zhang, Z. Unified vision-language-action model, 2025d. URL <https://arxiv.org/abs/2506.19850>.
- Wen, J., Zhu, M., Zhu, Y., Tang, Z., Li, J., Zhou, Z., Li, C., Liu, X., Peng, Y., Shen, C., et al. Diffusion-vla: Scaling robot foundation models via unified diffusion and autoregression. *arXiv preprint arXiv:2412.03293*, 2024.
- Wen, J., Zhu, Y., Li, J., Tang, Z., Shen, C., and Feng, F. Dexvla: Vision-language model with plug-in diffusion expert for general robot control. *arXiv preprint arXiv:2502.05855*, 2025a.
- Wen, J., Zhu, Y., Li, J., Zhu, M., Tang, Z., Wu, K., Xu, Z., Liu, N., Cheng, R., Shen, C., et al. Tinyvla: Towards fast, data-efficient vision-language-action models for robotic manipulation. *IEEE Robotics and Automation Letters*, 2025b.
- Wu, K., Hou, C., Liu, J., Che, Z., Ju, X., et al. Robo-mind: Benchmark on multi-embodiment intelligence normative data for robot manipulation. In *Robotics: Science and Systems (RSS) 2025*. Robotics: Science and Systems Foundation, 2025.
- Wu, P., Shentu, Y., Yi, Z., Lin, X., and Abbeel, P. Gello: A general, low-cost, and intuitive teleoperation framework for robot manipulators, 2024. URL <https://arxiv.org/abs/2309.13037>.
- Yang, Z., Yu, X., Chen, D., Shen, M., and Gan, C. Machine mental imagery: Empower multimodal reasoning with latent visual tokens. *arXiv preprint arXiv:2506.17218*, 2025.
- Ye, A., Zhang, Z., Wang, B., Wang, X., Zhang, D., and Zhu, Z. Vla-r1: Enhancing reasoning in vision-language-action models. *arXiv preprint arXiv:2510.01623*, 2025.
- Zawalski, M., Chen, W., Pertsch, K., Mees, O., Finn, C., and Levine, S. Robotic control via embodied chain-of-thought reasoning, 2025. URL <https://arxiv.org/abs/2407.08693>.
- Zhai, X., Mustafa, B., Kolesnikov, A., and Beyer, L. Sigmoid loss for language image pre-training. In *International Conference on Computer Vision (ICCV)*, 2023.
- Zhang, J., Guo, Y., Hu, Y., Chen, X., Zhu, X., and Chen, J. Up-vla: A unified understanding and prediction model for embodied agent. *arXiv preprint arXiv:2501.18867*, 2025a.
- Zhang, W., Liu, H., Qi, Z., Wang, Y., Yu, X., Zhang, J., Dong, R., He, J., Wang, H., Zhang, Z., et al. Dreamvla: a vision-language-action model dreamed with comprehensive world knowledge. *arXiv preprint arXiv:2507.04447*, 2025b.
- Zhao, Q., Lu, Y., Kim, M. J., Fu, Z., Zhang, Z., Wu, Y., Li, Z., Ma, Q., Han, S., Finn, C., et al. Cot-vla: Visual chain-of-thought reasoning for vision-language-action models. In *Proceedings of the Computer Vision and Pattern Recognition Conference*, pp. 1702–1713, 2025.
- Zhou, G., Dean, V., Srirama, M. K., Rajeswaran, A., Pari, J., Hatch, K., Jain, A., Yu, T., Abbeel, P., Pinto, L., Finn, C., and Gupta, A. Train offline, test online: A real robot learning benchmark, 2023a.
- Zhou, J., Wang, J., Ma, B., Liu, Y.-S., Huang, T., and Wang, X. Uni3d: Exploring unified 3d representation at scale, 2023b. URL <https://arxiv.org/abs/2310.06773>.

A. Large Scale Pre-training Datasets

To ensure LaST₀ inherits a robust foundation of motor primitives and physical common sense, we curated a diverse corpus of 400K trajectories (28M frames) from the Open-X-Embodiment (Open X-Embodiment Collaboration et al., 2023), DROID (Khazatsky et al., 2024), and RoboMIND (Wu et al., 2025) repositories. Table 3 lists the detailed proportions of each dataset used. Notably, beyond following prior VLA works in applying data quality filtering (Kim et al., 2024; Liu et al., 2025b), we additionally ensure that all robot state annotations are accurate and physically consistent. Specifically, to empower the slow reasoning expert with early geometric awareness, we utilized VGGT (Wang et al., 2025a) to generate synthetic 3D point clouds for all pretraining frames. These generated point clouds serve as the initial 3D geometric latent (z^p) inputs within the LaST CoT, allowing the model to learn spatial occupancy and environment dynamics even in the absence of real-world depth sensors during pretraining. This strategic alignment ensures a seamless transition to the full multimodal LaST CoT space during fine-tuning. This pretraining stage optimizes the model on broad robotic datasets to establish a shared representation space, enabling seamless interaction between reasoning and execution within the unified VLA framework.

Table 3. **Datasets used for pre-training.** The names of selected datasets for large-scale pretraining and their sampling ratios (%).

| Dataset | Ratio (%) |
|---|-----------|
| BC-Z (Jang et al., 2022) | 7.54 |
| Berkeley Autolab Ur5 (Chen et al.) | 0.35 |
| BridgeV2 (Ebert et al., 2022; Walke et al., 2023) | 20.93 |
| CMU Stretch (Mendonca et al., 2023) | 0.02 |
| DLR Sara Grid Clamp (Padalkar et al., 2023) | 0.02 |
| DROID (Khazatsky et al., 2024) | 4.82 |
| Dobb-E (Shafiullah et al., 2023) | 0.18 |
| FMB Dataset (Luo et al., 2023) | 1.50 |
| Fractal (Brohan et al., 2022) | 13.67 |
| Furniture Bench (Heo et al., 2023) | 0.09 |
| Jaco Play (Dass et al., 2023) | 0.19 |
| Kuka (Kalashnikov et al., 2018) | 20.22 |
| Language Table (Lynch et al., 2023) | 7.72 |
| Maniskill (Gu et al., 2023) | 5.26 |
| Nyu Franka Play (Cui et al., 2022) | 0.24 |
| Robo-Net (Dasari et al., 2020) | 11.53 |
| Roboset (Kumar et al., 2023) | 3.21 |
| RoboTurk (Mandlekar et al., 2018) | 0.70 |
| Stanford Hydra (Belkhale et al., 2023) | 0.20 |
| Taco Play (Rosete-Beas et al., 2022; Mees et al., 2023) | 1.26 |
| Toto (Zhou et al., 2023a) | 0.17 |
| Utokyo Pr2 Fridge (Oh et al., 2023) | 0.01 |
| Utokyo Pr2 Tabletop (Oh et al., 2023) | 0.04 |
| Utokyo Xarm Pap (Matsushima et al., 2023) | 0.04 |
| RoboMIND (Wu et al., 2025) | 0.2 |

B. Real-world Set-up

B.1. Franka robot setups

The physical deployment of LaST₀ utilizes a modular robotic infrastructure designed to provide the rich multi-modal feedback necessary for deliberative reasoning and responsive control. As shown in Fig. 7a, for single-arm configurations,

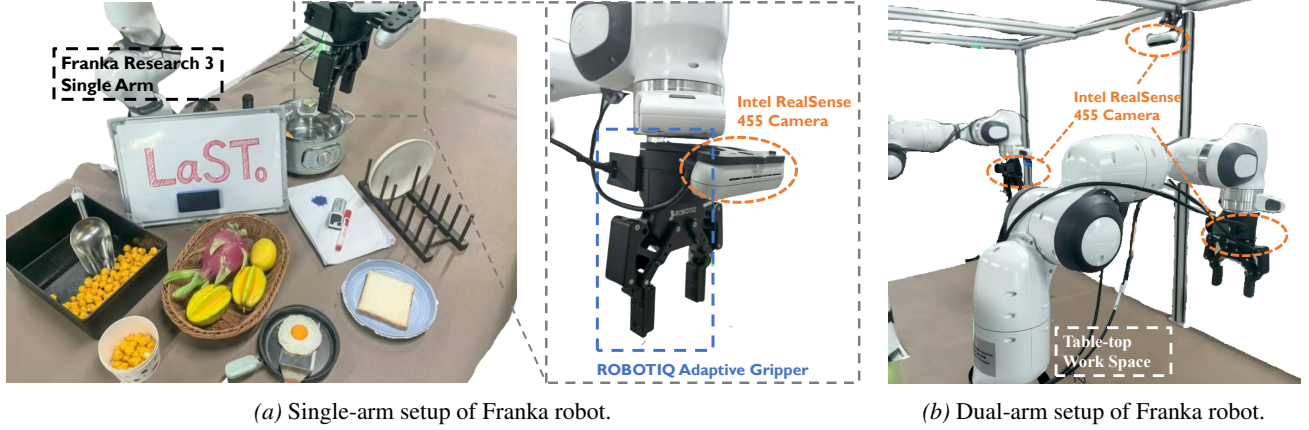


Figure 7. Robot experiment setups of Franka Panda Arms.

we deploy a Franka Research 3 (FR3) manipulator paired with a ROBOTIQ adaptive gripper. The perceptual backbone consists of two Intel RealSense D455 cameras: a stationary third-person unit providing the right-front perspective required for the Slow Reasoning Expert’s spatio-temporal planning, and a wrist-mounted unit for high-frequency visual servoing.

As shown in Fig. 7b, in dual-arm scenarios, the architecture scales to two parallel FR3 arms with identical end-effector and haptic configurations. This bimanual setup expands the perceptual suite to a three-camera array, including an additional front view camera and dual wrist cameras to capture the complex, synchronized spatio-temporal dependencies essential for collaborative manipulation. All demonstrations were collected using the Gello platform (Wu et al., 2024), with 200 high-quality demonstrations per task. The robot arm and gripper control methods are described in the preliminaries of the main paper.

B.2. AgileX mobile manipulation setups

As shown in Fig. 8a, for AgileX Mobile Manipulation tasks, we employ the AgileX Cobot Magic platform, including four AgileX Piper arms and a Tracer mobile base. Each of the puppet arms are equipped with an Orbbec Dabai camera at its wrist to capture RGB images. In addition, an Intel RealSense 515 camera is used on the robot’s head view to obtain head observations. Three views of RGB images are used in total during training. For this platform, we adopt a unified 20-DoF action space $\mathbf{a}_m \in \mathbb{R}^{20}$. The first 14 dimensions represent the 6-DoF joint position (delta angles) and 1-DoF gripper state for the right (R) and left (L) arms, respectively. The final 6 dimensions control the mobile chassis, consisting of 3-DoF linear velocities and 3-DoF angular velocities:

$$\mathbf{a}_m = [\Delta\theta_{1:6}^R, g^R, \Delta\theta_{1:6}^L, g^L, \mathbf{v}_{lin}, \boldsymbol{\omega}_{ang}] \in \mathbb{R}^{20} \quad (3)$$

B.3. TienKung humanoid dexterous hand setups

As shown in Fig. 8b, for the TienKung Dexhand Manipulation task, we employ the TienKung 2.0 platform, which consists a TienKung 2.0 Humanoid Robot, two ROHand AP001 R01 Dexterous hands and a Orbbec Gemini 336 camera on its head. Only one RGB image is used as image observation during training. We adopt a unified 26-DoF action space $\mathbf{a}_d \in \mathbb{R}^{26}$. This vector concatenates control signals for the right and left arms sequentially, with each arm accounting for 13 dimensions. Specifically, within each 13-DoF block, the first 7 dimensions represent the delta joint angles of the arm, followed by the 6 dimensions for the delta joint angles of the dexterous hand:

$$\mathbf{a}_d = [\Delta\theta_{1:7}^R, \Delta\phi_{1:6}^R, \Delta\theta_{1:7}^L, \Delta\phi_{1:6}^L] \in \mathbb{R}^{26}$$

Notably, to accommodate changes in action dimensions, only the noised-action MLP and the final MLP requires retraining to project noise to LLM’s embedding space and project hidden state to final action, respectively.

C. Self Collected Data

Building upon our real-world experiment setup, we evaluate LaST₀ across 10 representative tasks. These scenarios are specifically designed to validate the model’s ability to balance high-level deliberative reasoning via the LaST CoT with responsive, high-frequency execution.

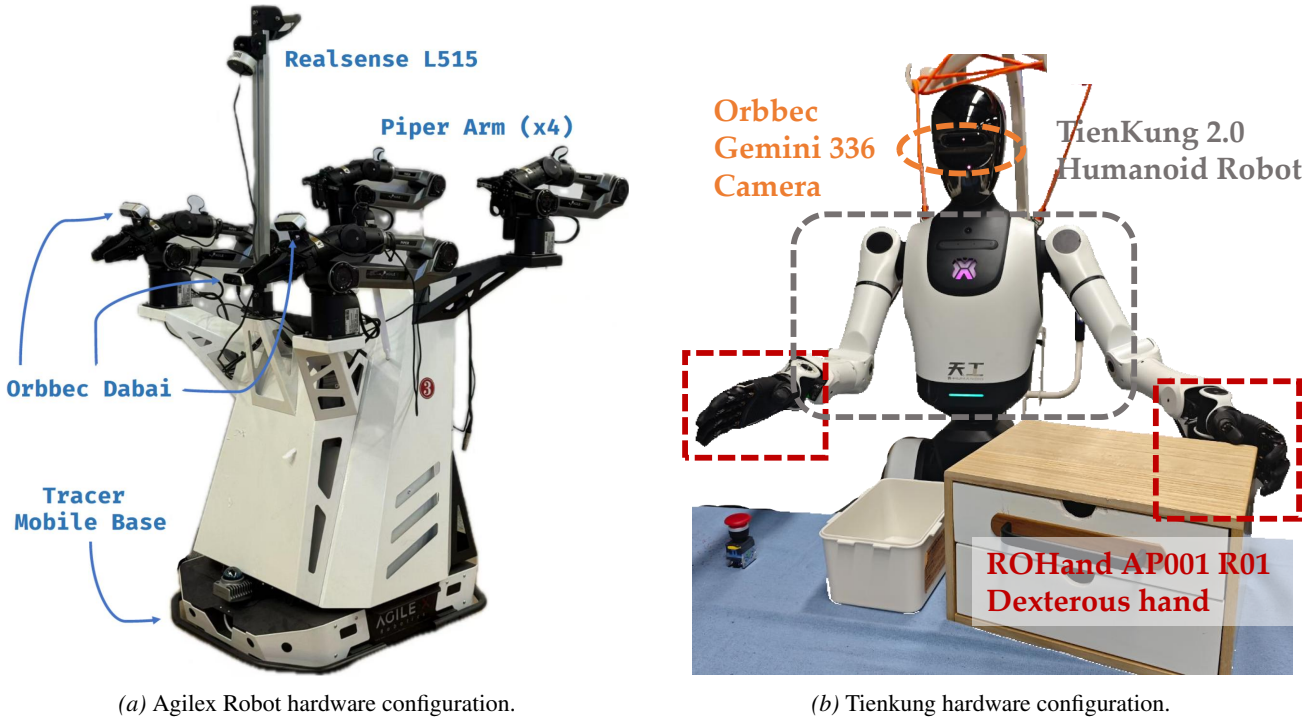


Figure 8. Robot experiment setups of Agilex Mobile Manipulation Tasks and TienKung Dexterous hand Manipulation Tasks.

C.1. Franka Emika Panda Arms

1. *Wipe whiteboard.* This task requires the robot to pick up an eraser on the table and clear colored blocks through visual recognition. Success depends on the model’s ability to maintain a stable spatial trajectory and ensure the erasing path accurately covers the target blocks.
2. *Press stamp.* The robot is required to establish a stable grasp on a stamp and execute a vertical press onto paper. This task evaluates the model’s ability to maintain a consistent execution plan even when the critical contact point is visually occluded during the final press.
3. *Place dish on rack.* This task requires the robot to grasp a plate and perform a large 6-DoF rotation to insert it into a narrow rack. This demands highly accurate spatial perception and the ability to predict complex rotational trajectories for upright placement.
4. *Place egg on bread.* This task requires the robot to pick up the spatula, lift the egg, and place the egg onto the bread. The model must reason about the precise relative positioning between the spatula tip and the pan to slide under and lift the egg without failure.
5. *Scoop popcorn into bowl.* This collaborative task involves one arm scooping with a bucket while the other arm holds a bowl, then placing the bowl with popcorns on the plate. It validates the model’s capacity for precise temporal synchronization and spatial coordination between two independent action streams.
6. *Open pot pick corn.* A long-horizon sequence involving lid removal, object retrieval, and lid replacement. This task evaluates the model’s planning depth and collision-avoidance capabilities within a restricted workspace requiring seamless bimanual interaction.

C.2. Agilex Mobile Manipulation Tasks

1. *Arrange dishes.* This task requires the robot to move front to the table and arrange two dishes collaboratively with two arms. Completing the task requires coordination between the chassis position and the robotic arm position, demonstrating the model’s multi-dimensional control capabilities for long-horizon planning.
2. *Sort spoons.* The robot is required to pick up two spoons with two arms respectively and move to the cabinet, then place

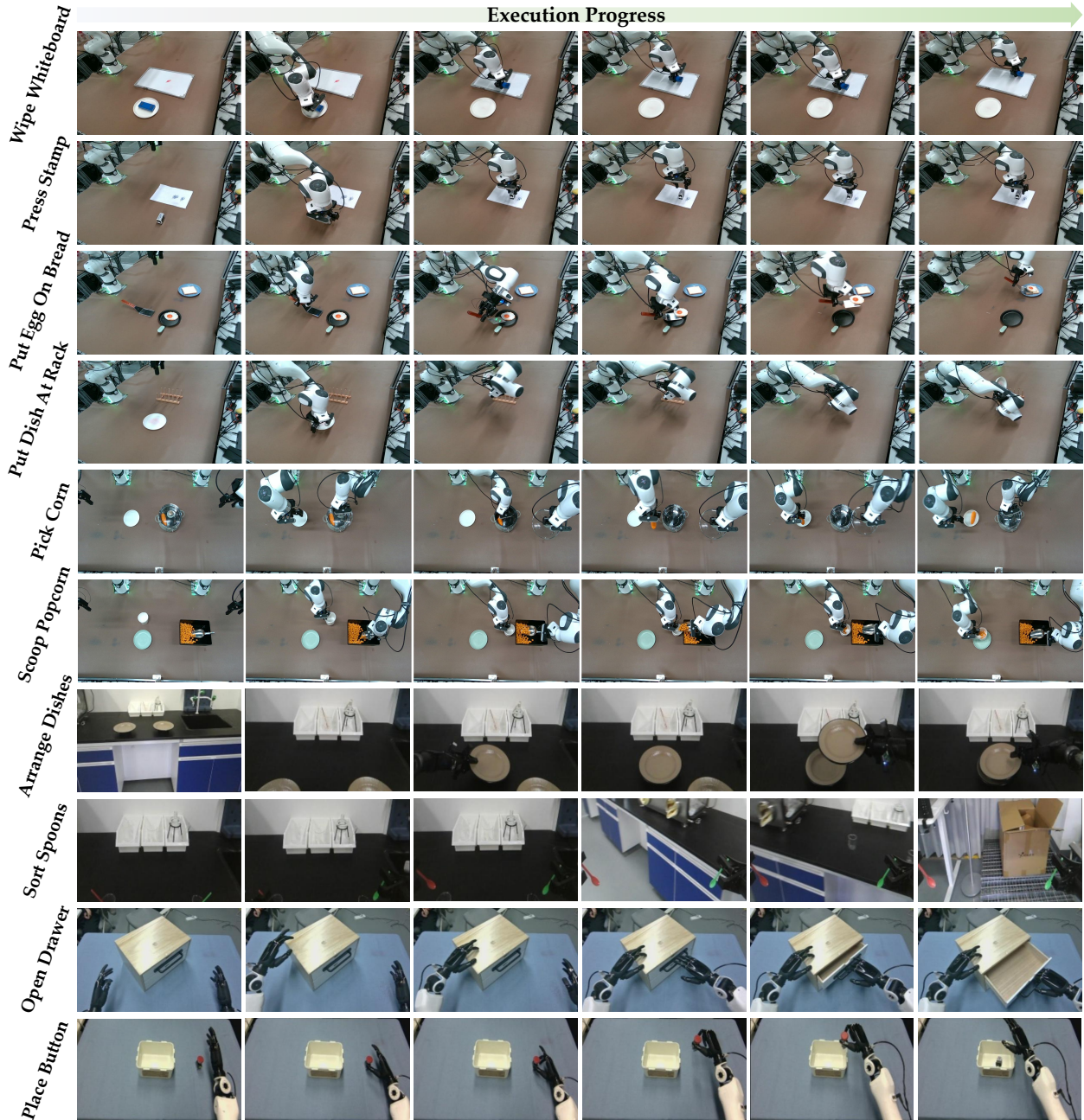


Figure 9. Visualization of complete task execution processes by real-world tasks (from left to right).

the spoons in it. The process of picking up the spoons requires the model to have precise manipulation capabilities, while the subsequent movement requires the model to understand spatial relationships in an open environment.

C.3. Tiengkung Humanoid Dexterous Hand Task

1. *Open drawer.* This task requires the robot to handle the drawer with the left hand and open drawer with the right hand. The right hand needs to be precisely positioned on the drawer handle to successfully pull out the drawer, requiring a high degree of fine-grained manipulation of the model.

2. *Place button.* This task requires the robot to pick up the button with dexterous hand and place it into the box. The model needs to accurately handle the relationship between each finger and the complex surface structure of the object.

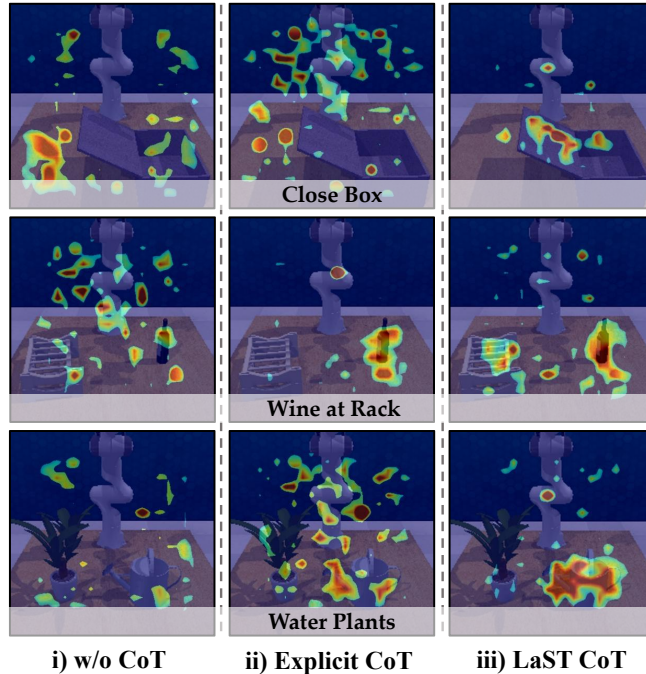


Figure 10. **Visualization of attention heatmaps.** We visualize the attention heatmaps from the final layer of LaST₀ on RL Bench observations. The red area indicates the regions with high attention weights, highlighting the model’s focus on task-relevant entities.

D. Additional Visualization

Additional Real-World Visualizations. Fig. 9 illustrates representative task executions across single-arm and dual-arm settings, mobile manipulation tasks and dexterous hand tasks. We observe that LaST₀ produces smooth and continuous motions, particularly in precise actions such as surface wiping, spatula-mediated placement, and bimanual scooping. This behavior is enabled by the proposed LaST CoT and dual-system design, where a low-frequency reasoning expert provides temporally coherent latent guidance, while the action expert operates at a higher control frequency, allowing rapid and fine-grained response to environment dynamics. We also verify the model’s closed-loop capability: for example, when new marks are continuously drawn on the whiteboard during manipulation, the robotic arm can persistently perform the erasing action.

Additional Attention Visualizations. As shown in Fig. 10, we compare the attention heatmaps of LaST₀ against variants without CoT and with explicit CoT (CoT-VLA) on several RL Bench tasks. While the No-CoT and Explicit CoT variants fail to attend to the critical dynamics of the scene, often focusing on irrelevant background textures, LaST₀ demonstrates precise semantic alignment. It explicitly targets the interaction between the robot arm and the object, highlighting its superior spatio-temporal understanding capabilities.

E. Failure Case Analysis

For different scenarios, we recorded three typical failure cases, as shown in Fig. 11, where the red boxes indicate the specific locations and results of the failures.

- 1) In the first case, the FR3 arm is required to use an eraser to wipe a pattern off a whiteboard, but due to an error in the **manipulation height**, it did not descend to a height that was completely flush with the whiteboard, resulting in the pattern not being completely erased. The lack of visual feedback during the erasing process regarding the presence or absence of the pattern increases the probability of this happening.
- 2) The second case demonstrates **object collision** during a dual-arm collaborative task. During the process of the right arm placing the second plate onto the first one, the two plates collided, causing the first plate to shift from its original position. This occurred because the model incorrectly estimated the required height and position for stacking the plates.
- 3) The failure in the third case in the dexterous manipulation task is a typical case of **incorrect manipulation position**. The model did not move the hand forward enough to grasp the drawer handle, leading to a failed pull.

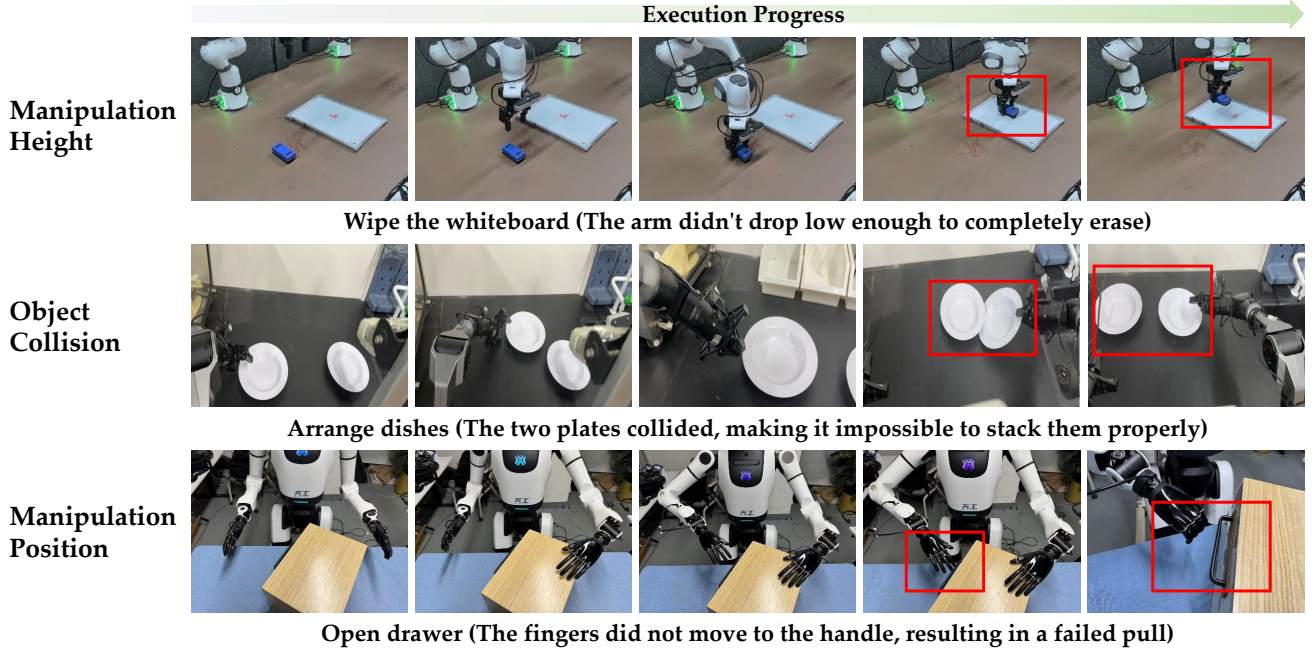


Figure 11. Visualization of failure cases on different robot platforms, the task progresses from left to right, and red box highlights the failure positions.

F. Additional Method Details

F.1. Additional Preliminaries

Robotic CoT Reasoning. To bridge the gap between high-level visual observations and low-level control, recent VLA methods introduce an intermediate CoT variable \mathcal{Z} . This formulation decomposes the policy distribution into a reasoning stage (predicting \mathcal{Z}) and an execution stage (predicting \mathbf{a} conditioned on \mathcal{Z}):

$$p(\mathbf{a}, \mathcal{Z} \mid I_t, l) = p(\mathbf{a} \mid \mathcal{Z}, I_t, l) \cdot p(\mathcal{Z} \mid I_t, l)$$

Existing methods typically adopt an explicit CoT paradigm, where \mathcal{Z} consists of discrete natural language tokens (Li et al., 2024a) or image tokens (Zhao et al., 2025; Zhang et al., 2025a). While interpretable, these approaches confine reasoning to the linguistic space of LLMs, which struggles to represent ineffable physical attributes and incurs inference latency due to explicit decoding. In this paper, we propose a new latent CoT paradigm for the robotic domain. Unlike explicit CoT, we define $\mathcal{Z} = \{\mathbf{z}_1, \dots, \mathbf{z}_k\}$ as a sequence of continuous embeddings in a high-dimensional latent space. In our framework, the latent variable \mathcal{Z} is trained to autoregressively predict future dynamics, including latent representations of 2D images, 3D point clouds, and robot proprioceptive states, thereby modeling the physical world in a compact space.

F.2. Dual-System Coordination

Inference via KV Cache. During inference, the Key-Value states computed by the slow expert (encapsulating the Latent CoT) are cached in memory. During intermediate fast-control steps, the acting expert only encodes the current observation and attends to the frozen latent CoT cache, effectively retrieving the CoT tokens with $O(1)$, without re-invoking the slow reasoning process. This approach eliminates repetitive decoding, allowing our model to achieve an inference speed of 15.4 Hz on a single RTX 4090 GPU when operating with a 1:4 fast-slow frequency ratio. In particular, the slow reasoning expert runs at 12.7 Hz, while the fast acting expert runs at 22.1 Hz, resulting in 15.4 Hz in total each 4 steps.